Stony Brook University

Synthetic Studies of Phosphate Based Ceramic Materials

A Thesis Presented

by

Yiran Zhao

to

The Graduate School

in Partial Fulfillment of the

Requirements

for the Degree of

Master of Science

in

Chemistry

Stony Brook University

May 2017

Stony Brook University

The Graduate School

Yiran Zhao

We, the thesis committee for the above candidate for the Master of Science degree, hereby recommend acceptance of this thesis.

Peter Khalifah – Thesis Advisor

Associate Professor Department of Chemistry

Benjamin S. Hsiao – Chairperson of Defense

Distinguished Professor Department of Chemistry

Amy C. Marschilok – Third Member

Research Professor Department of Chemistry

This thesis is accepted by the Graduate School

Charles Taber

Dean of the Graduate School

Abstract of the Thesis

Synthetic Studies of Phosphate Based Ceramic Materials

by

Yiran Zhao

Master of Science

in

Chemistry

Stony Brook University

2017

Phosphate based ceramics are widely used in the field of energy materials, where they have been used both as solid state ionic conductors and as electrode materials. Two kinds of phosphate based ceramics: NASICONs (Na Super Ion Conductors) and alpha-cristobalite form $AlPO_4$ were synthesized and analyzed in this work.

Phosphate based NASICONs materials, which have the general formula: $A_{3-x}M_2(PO_4)_3$, represent the first known family of Na superionic conductors, and for this reason have found use as solid state electrolytes. More recently, lithium-substituted NASICON-structured materials have been identified as candidate electrolytes for solid state lithium ion batteries. Various approaches for the synthesis of NASICON-type compounds $Li_{1.5}Al_{0.5}Ti_{1.5}(PO_4)_3$ and $Na_{1.5}Al_{0.5}Ti_{1.5}(PO_4)_3$ were pursued in this work. A variety of experimental conditions (different reaction containers, different reaction atmospheres, different reaction precursors, etc.) were tried to overcome

limitations of the high reactivity of samples with crucibles during synthesis procedures. X-ray diffraction techniques were used to identify and quantify product and impurity phases.

A second phosphate based ceramic material investigated in the course of this work is AlPO4 with the alpha-cristobalite structure. It is known that SiO_2 with the alpha-cristobalite structure is a rare example of a ceramic with a negative Poisson's ratio. Polycrystalline alpha-cristobalite $AlPO_4$ was synthesized to investigate whether this predicted behavior can indeed be observed. Although the many phase transitions between different polymorphs of $AlPO_4$ complicate the synthesis of the desired alpha-cristobalite form, good methods for preparing dense pellets of this phase were developed.

Table of Contents

List of Figures/Tables

Acknowledgments

First and foremost, I would like to thank my advisor, Dr. Peter Khalifah, for giving me an opportunity to discover this interest in solid state chemistry research. His never-ending effort, patience, guidance and support helped me to finish my research program.

I would like to thank Dr. John Parise and his group member Shen Tu for helping me collecting XRD data while our X-ray diffractometer was down. I would also like to thank my group mate Liang Yin for teaching and inspiring me with my research, and thanks Zhuo and Gerry for their friendship and help. They have been very supportive of me throughout this experience, and have helped me countless times throughout the lab.

Lastly, I would like to thank my family and friends. Their constant support and words of encouragement fuel me to pursue my dreams and to continue to strive for better.

Chapter 1. Introduction and background

1.1 Phosphate based ceramics

The origin of ceramics can date back to the beginning of human civilization. Early ceramics are used to make tools for hunting, cooking and self-defense. As the deepening of research on ceramics, many properties were studied such as mechanical properties, electrical properties and optical properties. In industrial areas, phosphate based ceramics and glasses are widely used as binders, refractories. In the medical field, the use of those materials containing coatings for protection against oxidation, corrosion, and prostheses for hard tissues. [1] Phosphate based ceramics are considered as one of the major inorganic room-temperature setting materials for nuclear, structural, dental and prosthetic applications. [2] Phosphate based ceramics are a series of ceramics consist of phosphate groups and metal, or non-metal atoms. Phosphate groups always form tetrahedra in the structures of crystalline phosphate ceramics. This configuration also attracts researchers to make more efforts on the structural study of phosphate ceramics.

1.2 NASICONs and batteries

1.2.1 Batteries and electrochemical storage

The growth of world population is always a big problem that people need to take account at any time. The median estimate for future world population reaches 9.7 billion in 2050 and 11.2 billion in 2100. Growing populations consume more and more energy. The increasing demands of energy make traditional energy resources scarcer and harder to extract. This leads to the exploitation of renewable energy. Many attempts were made by using wind power, hydropower,

solar energy, geothermal energy and bioenergy. There are many limitations during the exploration of new energy such as technical challenges and many restrictions on geographical characters, the focus has been changed to batteries for energy storage.

As the essential component of most electrical devices, batteries become the indispensable part of our daily life. The battery is a device used to store electrical energy. It powers our cell phones, laptops, flashlights, remote controls and is also widely used in vehicle devices. Compared to fossil fuel, batteries have the advantage of delivering energy.

Batteries can be categorized into two types: primary batteries and secondary batteries. Primary batteries are not designed to be recharged and reused, and the materials in the cell are irreversibly changed once discharge occurs. Conversely, secondary batteries, also are called rechargeable batteries, can charge and discharge reversibly over many operation cycles.

A battery consists of an anode, a cathode, and electrolyte. The electrolyte is always used as the separator between two oppositely charged electrodes. When the battery charges and discharges, ions shuttle between the anode (negative electrode) and cathode (positive electrode). For a primary battery, the anode is typically the ion donor, and the cathode is typically the ion acceptor. However, the roles may reverse when it comes to secondary batteries, when the battery charges and current flow from the anode to cathode. The electrolyte between two electrodes is filled with electrolyte which provides a mechanism for ion transport. Figure 1 shows the principle of a secondary battery. To avoid resistive losses batteries required that electrodes must be both good ionic and electronic conductors. Carbon black and binder are added into the electrode materials. For this reason, carbon black is used to increase the electronic conductivity and a binder keeps the electrode and carbon together.

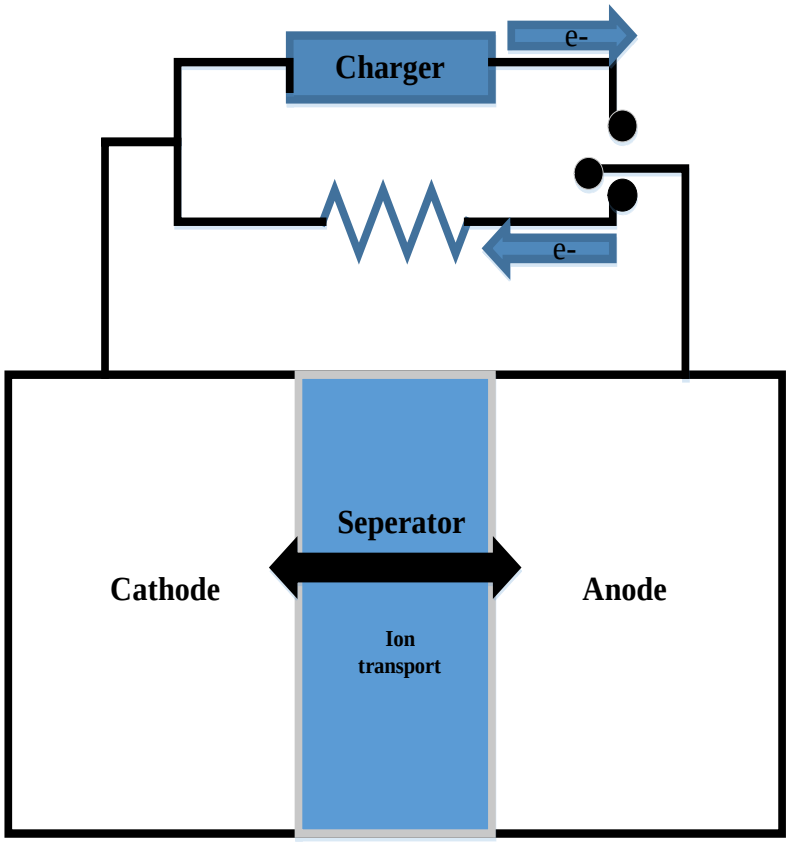

Figure 1. Diagram of a rechargeable battery

To make a battery conductive, the electrolyte promotes the movement of ions from the cathode to the anode when charging and in reverse on discharge. At present, many kinds of electrolytes were studied. $LiClO_4$ dissolved in propylene carbonate is a kind of common liquid electrolyte used in Lithium batteries. However, this suffers from certain shortcomings like limited temperature range of operation and electrode corrosion by electrolyte solution and unsuitable shapes. In some cases, the solid electrolyte may overcome these disadvantages.

There are mainly two kinds of solid electrolyte have been studied. Solid polymer electrolyte is a kind of solid electrolyte that can work as the separator between two electrodes, and they can also retain contact over an interface of electrode and electrolyte during modest changes of the electrode volume with the state of charge of the battery. One example of low cost, nontoxic lithium ion

polymer electrolyte is polyethylene oxides (PEOs) containing a lithium salt ($LiPF_6$ or $LiAsF_6$).[2-4] But the lithium ion conductivity of solid polymer electrolyte is still comparable to that of the carbonate electrolyte. [5] Inorganic solid electrolyte was widely studied on lithium ion conducting material, because they have good both lithium ion and electronic conductivity, and chemical stability over temperature in the battery under high power. [6-9]

1.2.2 NASICON-type materials

In 1976, a framework structure $Na_{1+x}Zr_2P_{3-x}Si_xO_{12}$ was proposed, which provides three-dimensional migration tunnels for Na^+. This kind of structure was named as NASICON. [10] These compounds are considered as a series of structurally isomorphous 3D framework compounds possessing high conductivity.

The general formula of NASICON is $AMM'X_3O_{12}$. In this formula, A can be occupied by some cations like Na^+, Li^+, M and M' sites can be occupied by some transition metal ions to balance the charge suitably. X usually is occupied by P or Si. Depending on the composition, the crystal structure can be different. For many NASICONs which are orthorhombic, as is shown in Figure 2, the framework is built of XO_4 linked by corners to MO_6 octahedron group and, therefore, each MO_6 octahedron shares each corner with a different XO_4 group.

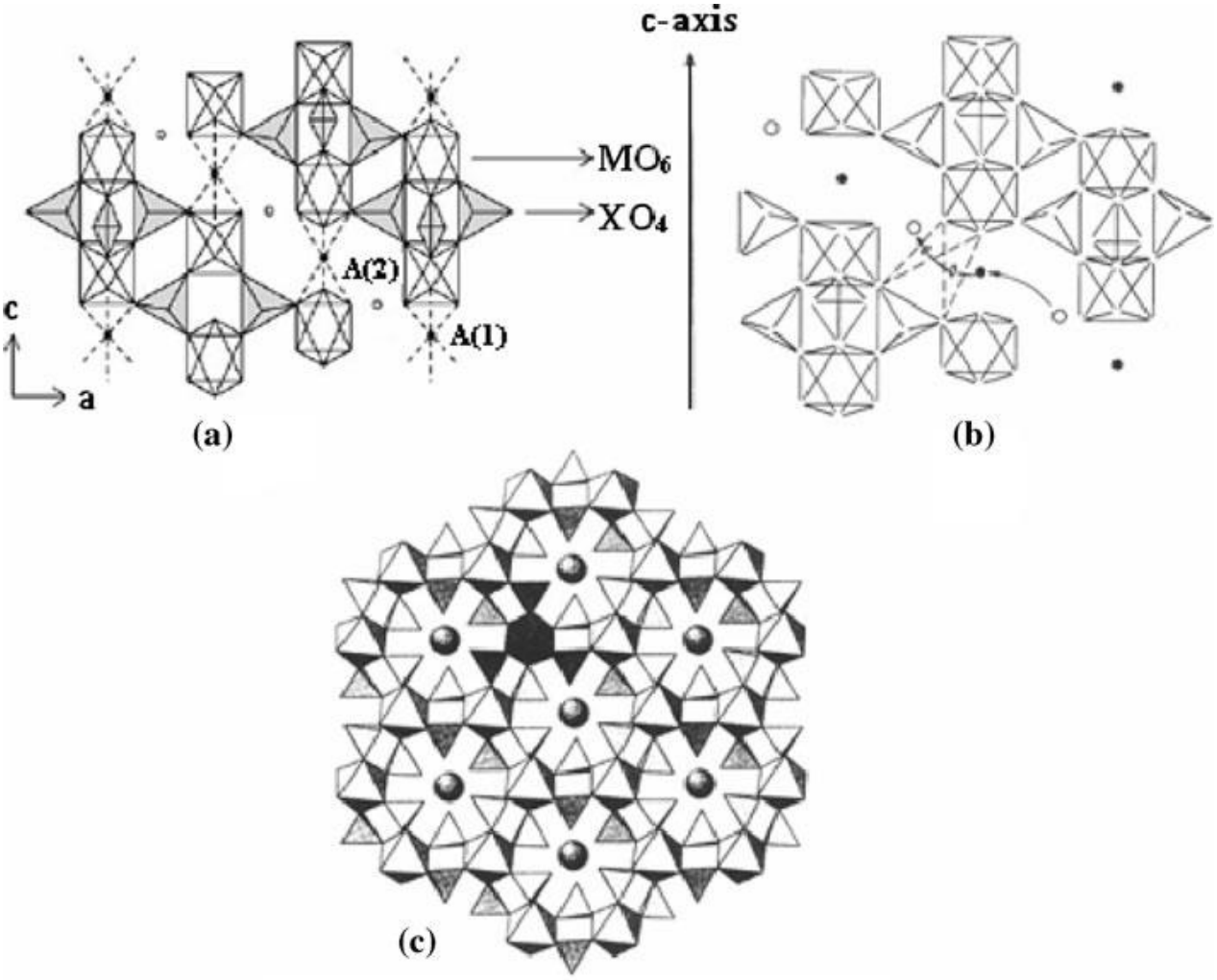

Figure 2. The structure of Nasicon [11]

Much research has been done on its application on electrode materials. A good example is $Li_3Ti_2(PO_4)_3$; it has been studied as a cathode material. [12] Besides, metal insertion studies on some NASICONs like $NaZr_2P_3O_{12}$ type materials are reported. [13-16] And NASICON-type materials always show low thermal expansion property which was also exploited, like some this kind of materials are considered as attractive candidates for thermal shock, telescope mirrors, high energy lasers and precision optics ovenware. [17,18]

There are mainly two synthesize methods: sol-gel method and solid state method. Compare to the sol-gel method, solid state method needs a higher temperature, but much easier to do. In this work, solid state method was used in the synthesis of NASICONs.

1.3 Alpha- cristobalite $AlPO_4$ and Negative Poisson's ratio material

1.3.1 Negative Poisson's ratio material

Poisson's ratio, which is also called the Poisson coefficient, is a term that describes the deformation of materials when compressed or stretched. Poisson's ratio is defined as the ratio of transverse contraction strain to longitudinal extension strain in the direction of stretching force. For the most common materials, they become thinner in cross section when stretched, so the Poisson's ratio is positive. Materials such as normal polymer foams or cellular solids have a positive Poisson's ratio. Figure 3 shows how materials change when stretched or pressed.

Assuming that the material is stretched or compressed along the axial direction (the x-axis in the below diagram), the equation can be:

$$\nu = -\frac{d\varepsilon_{trans}}{d\varepsilon_{axial}}$$

where

ν is the resulting Poisson's ratio,

$d\varepsilon_{trans}$ is transverse strain (negative for axial tension (stretching), positive for axial compression)

$d\varepsilon_{axial}$ is axial strain (positive for axial tension, negative for axial compression).

Structures or materials which have a negative Poisson's ratio, also called auxetics, become thicker perpendicular to the applied force when stretched like what's shown in Figure 4. This happens due to their unusual internal structure. Negative Poisson's ratio material can be single molecules, crystals, or a certain structure of macroscopic matter. Such structures and materials are expected to have high energy absorption and fracture resistance.

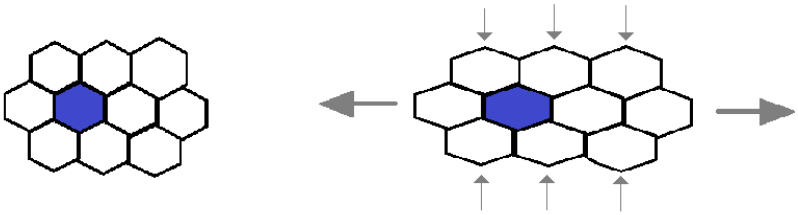

Figure 3. Normal materials [19]

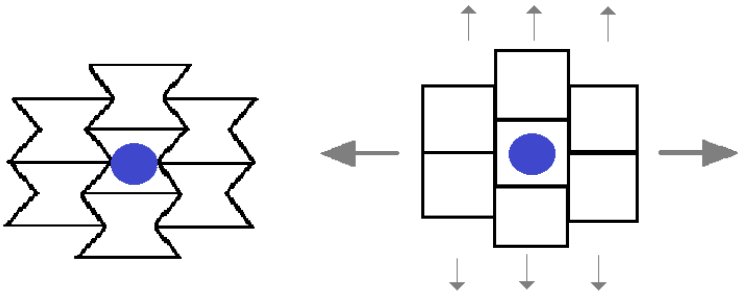

Figure 4. Auxetic material [19]

The earliest negative Poisson's ratio material was published in Science in 1987. It was shown that a foam structure which exhibits a negative Poisson's ratio. Since then, more and more research was done on this kind of materials. [20]

Alpha-cristobalite, a low-density polymorph of SiO_2, was found showing an unusual elastic behavior of negative Poisson's ratio in 1999. [21] Since some essential properties such as crystal structure, polymorphism, melting point and mechanical behavior are very nearly the same in $AlPO_4$ and SiO_2, one could expect that α-cristobalite $AlPO_4$ is a kind of material that has negative Poisson ratio just like α-cristobalite SiO_2.

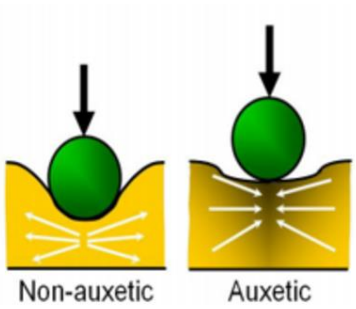

Figure 5. Differences between non-auxetic material and auxetic material

1.3.2 Close crystallographic relation between $AlPO_4$ and SiO_2

The structure of α-cristobalite $AlPO_4$ has been investigated in 1956. [22] The lattice consists of alternating AlO_4 and PO_4 tetrahedra. The space group of it is $C222_1$. $AlPO_4$ is isoelectronic with Si_2O_4. The most common phase of aluminum phosphate is berlinite, which is isomorphic with quartz. For the structure of berlinite, compare to that of quartz, silicon was replaced by Al and P and the AlO_4 and PO_4 tetrahedra alternate. The space group of berlinite is P321, of quartz is P622 and crystal structures are as follows (Figure 6).

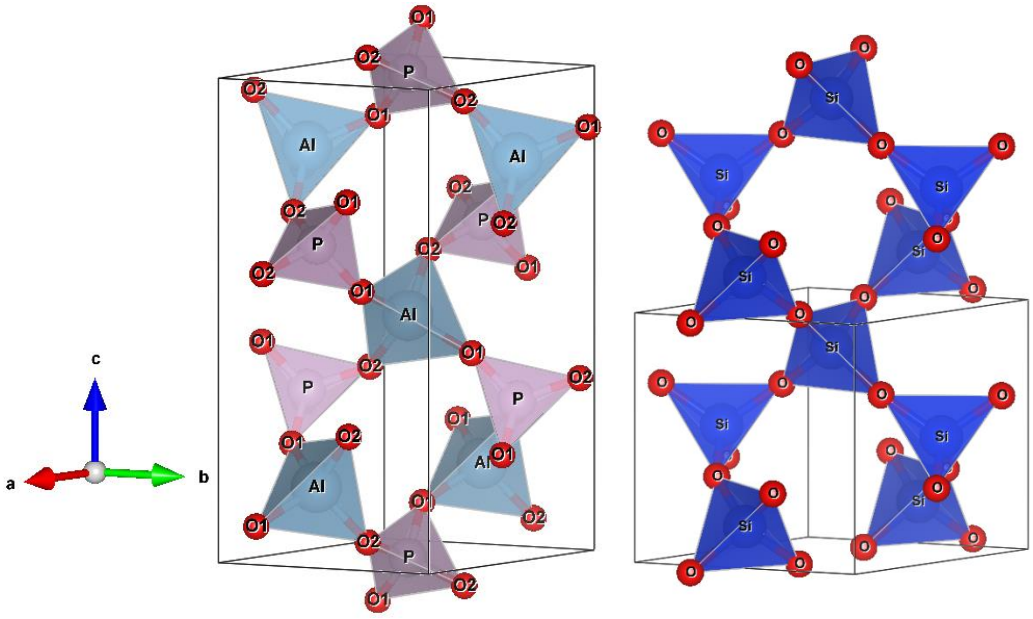

Figure 6. Structure of berlinite and quartz [23], [24]

Berlinite converts to tridymite and cristobalite form when heated which mirrors the behavior of SiO_2. The four forms of silica and their transformation relationship has been well studied. Following shows the synthesis condition of phase transformation diagram: [25]

$$\text{Quartz} \xleftrightarrow{870°C} \text{Tridymite} \xleftrightarrow{1470°C} \text{Cristobalite} \xleftrightarrow{1710°C} \text{Fused } SiO_2$$

$$\alpha \xleftrightarrow{573°C} \beta \qquad \alpha \xleftrightarrow{987°C} \beta_1 \xleftrightarrow{1033°C} \beta_2 \qquad \alpha \xleftrightarrow{1690-1740°C} \beta$$

The stability relationships of the AlPO4 polymorphs have also been studied and has a similar diagram with silica:

$$\text{Berlinite} \xleftrightarrow{815\pm4°C} \text{Tridymite Form} \xleftrightarrow{1025\pm50°C} \text{Cristobalite Form} \xleftrightarrow{>1600°C} \text{Fused } AlPO_4$$

$$\alpha \xleftrightarrow{586\pm2°C} \beta \qquad \alpha \xleftrightarrow{908\pm3°C} \beta_1 \xleftrightarrow{945°C} \beta_2 \qquad \alpha \xleftrightarrow{1240\pm5°C} \beta$$

1.3.3 Synthesis of α-cristobalite $AlPO_4$

Alpha-cristobalite $AlPO_4$ can be gained by phase transformation at a high temperature. Alpha-cristobalite $AlPO_4$ powder has been synthesized from high-purity α-Al_2O_3 and H_3PO_4. [26] A common and simple method is to heat amorphous or low-quartz type (berlinite) $AlPO_4$ to their cristobalite transition temperature and then allowed to cool rapidly to room temperature. The key point of this synthesis is quickly cooling process since the cristobalite form $AlPO_4$ would transform to other types especially tridymite form.

1.4 Experimental Techniques

1.4.1 Solid state synthesis

During this study, solid state synthesis is a simple and common used synthesis technique. In a typical sample preparation, a set of starting materials are appropriately mixed, sometimes including additives that may not be necessarily wanted in the product, by heating to a certain temperature and holding at that temperature for reaction. All of them are usually determined by experience. Sometime to avoid the evaporation at high temperature, appropriate excess amount certain precursor may be added.

Usually, after weighing those starting materials, we start alternating mixing and grinding. Fully grinding is necessary to achieve a homogenous mixture of precursors. In this research, there are some methods for mixing and ground starting materials. The first and simplest method is hand-grinding, which is grinding starting materials using a mortar and pestle. Grinding time depends on how many and how much those precursors have. The second method of grinding using the vibration ball mill, this kind of method is not suitable for a bit of sample and those that is easy absorbing water, because the agate ball may stick to the bottom once powder was absorbing water.

Contact of reactants may be increased by pelletizing the powders using a press. In this work, the Carver press was used to press pellets.

The reaction mixture should be removed and reground to bring fresh surfaces in contact, which may speed up the reaction and make the reaction more homogeneous. Reaction times are sometimes hours, but many ranges into several days or weeks (especially when single crystal growth) for a complete reaction with intermediate grinding.

For high-temperature reaction, different reaction conditions are determined by choice of furnace. Box furnace and high-temperature tube furnace are two kinds of common furnace. Box

furnace can be used for reactions in air or drying of the starting materials. High temperature tube furnace can be used for reactions required a certain gas atmosphere.

For crucibles, the containers for the reaction, they must be able to withstand high temperatures and be avoided to react with reactants. Conventional crucibles like silica, alumina, platinum, molybdenum, carbon crucible are used in different reactions.

1.4.2 Powder diffraction [27]

Powder X-ray diffraction has the benefit of the short data-collection time needed, small sample mass requirement, and the ability to recollect sample, is frequently used in solid state chemical analysis due to its practical laboratory uses.

The atoms form well-defined planes in every crystalline solid. Those well-defined planes and the reflection caused by them is useful when using X-ray diffraction. A scattering effect would be observed if the radiation wavelength is comparable to that of the space between planes. The spacing of the planes in a crystal is compatible with the wavelengths in the X-ray region.

Like visible light, X-ray is a type of electromagnetic radiation. However, X-rays have a much shorter wavelength. The X-rays entered the sample should then be reflected by the ions in any plane, and the reflected rays in each successive plane should interfere constructively. This is shown in Figure 7. The concept can also be shortly described as two rays reflect from two planes, the rays travel two different distances. Constructive interference will only occur if $2a=n\lambda$, or in figure 7 $d\sin\theta$, where n is an integer. Here gives the Bragg's law equation:

$$N\lambda=2d\sin\theta$$

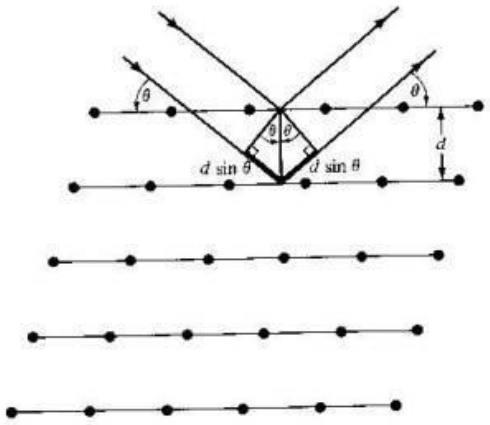

Figure 7. The behavior of the reflections of two planes from an X-ray beam.

In this work, the X-ray Bruker D8 Advance diffractometer was used for data collection and phase identification. X-ray Bruker D8 Advance diffractometer includes a Cu X-ray tube, a detector, and nine sample holders. X-rays are generated when a beam of electrons is accelerated to high energy and focused onto a metal target, in this case, copper. The high-energy beam knocks out an electron from the copper atoms allowing electrons to drop down from the outer shells. In this process, photons are emitted for the electrons to lose enough energy to get close to the nucleus. The photons emitted in this process are in the X-ray region. A nickel filter is used to cut off the K_β lines and only allow the $K_{\alpha 1}$ and $K_{\alpha 2}$ lines to be incident on the sample. Rigaku Ultima IV X-ray diffractometer was used to collect data because Bruker D8 Advance was down in last few months. The principles are similar to that of Bruker D8 Advance.

Chapter 2. NASICON-type material

Lithium cells are of widespread interest due to their high potential, and high energy density. Lithium-based solid electrolytes were also widely studied for solid lithium batteries. Lithium containing NASICON-type materials can be a good candidate of electrolytes in solid lithium batteries if the ionic conductivity properties are improved. $LiTi_2(PO_4)_3$ is the most studied in $LiM_2(PO_4)_3$ (*M*= Ti, Ge, Sn, Zr, Hf) system. [28] There might be an increase of $LiTi_2(PO_4)_3$ ionic conductivity for the partial substitution of Ti^{4+} by trivalent cations such as Ga^{3+}, Al^{3+}, In^{3+}, Ti^{3+}, Sc^{3+}, Y^{3+}, La^{3+}, Cr^{3+} or Fe^{3+}. [29-31] From previous research on the crystal structure of $LiTi_2(PO_4)_3$, as is shown in Figure 8, Ti^{4+} is six-coordinated and form an octahedron with six O around. Table 1 listed the ionic radius of Ti^{4+} and those trivalent cations mentioned above. In this case, Al^{3+} substitution is studied and $Li_{1.5}Al_{0.5}Ti_{1.5}(PO_4)_3$ was synthesized in this work.

Table 1. Crystal radius of 6-coordinated Ti^{4+} and its possible substitutions

Ions	Ti^{4+}	Al^{3+}	Fe^{3+}	Cr^{3+}	Ga^{3+}	In^{3+}	Ti^{3+}	Sc^{3+}	Y^{3+}	La^{3+}
Radius (Å)	0.745	0.675	0.69	0.755	0.76	0.76	0.815	0.88	1.04	1.172

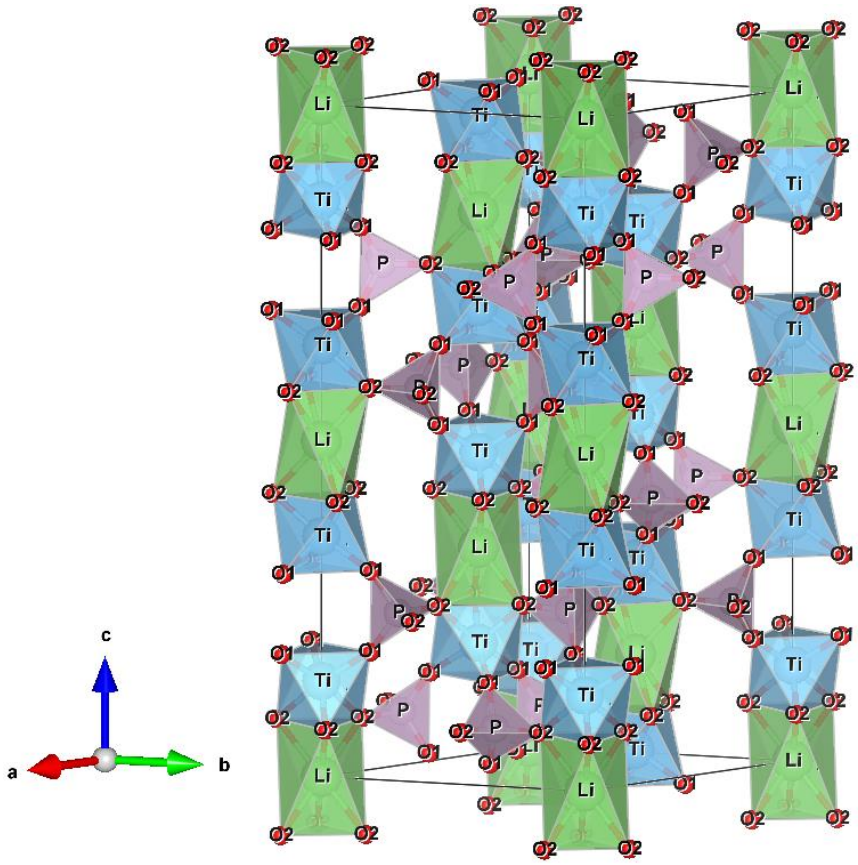

Figure 8. Crystal structure of $LiTi_2(PO_4)_3$ [32]

$Na_{1.5}Al_{0.5}Ti_{1.5}(PO_4)_3$ was also synthesized because it could be the precursor of $Li_{1.5}Al_{0.5}Ti_{1.5}(PO_4)_3$ by ion-exchange and all the starting materials of $Na_{1.5}Al_{0.5}Ti_{1.5}(PO_4)_3$ are nonharmful and cheap.

Another series of NASICON-type materials having the stoichiometry $NaZr_2P_3O_{12}$ (NZP), $Na_{1+x}Zr_2Si_xP_{3-x}O_{12}$ (NZP_Si), and $Na_{1+x}Al_xZr_{2-x}P_3O_{12}$ (NZP_Al) can also be used as both a solid electrolyte and electrode in sodium-based batteries. [33] ZrP_2O_7 should be a reasonable precursor of NZP, considering the composition of $NaZr_2P_3O_{12}$.

2.1 Experimental

2.1.1 $Na_{1.5}Al_{0.5}Ti_{1.5}(PO_4)_3$

$Na_{1.5}Al_{0.5}Ti_{1.5}(PO_4)_3$-a samples were prepared by using starting materials of Na_2CO_3, Al_2O_3 (Aluminum oxide, α-phase, 99.98%), activated TiO_2 (synthesized in lab), $(NH_4)_2HPO_4$ (Ammonium Phosphate Dibasic). Stoichiometric starting materials were heating to give the following reaction:

$$3/4\ Na_2CO_3 + 1/4\ Al_2O_3 + 3/2\ TiO_2 + 3\ (NH_4)_2HPO_4 \xrightarrow{\Delta} Na_{1.5}Al_{0.5}Ti_{1.5}(PO_4)_3\text{-A} + \text{gases}$$

In this case, activated TiO_2 was synthesized by hydrolysis of $Ti[OCH(CH_3)_2]_4$. Extra isopropanol (water to isopropanol is 1:4) was added to slow down the speed of deposition of TiO_2. The TiO_2 powder was then washed with water and dried at 140°C for 24 hours. TiO_2 powder was ready to use after that.

Stoichiometric mixtures of those starting materials were ground by vibrational ball milling for 3 hours. Thorough mixing is necessary. The mixture then was placed in a corundum crucible and heated to 350°C at the rate of 1°C/min in box furnace in air and kept it at that temperature for 6 hours. After the first heat treatment, powders were ground by ball milling for 1.5 hours. Then a second heat treatment was done at 650°C (at the same heating rate) for 8 hours for complete decomposition of Na_2CO_3 and $(NH_4)_2HPO_4$. Another 1.5-hour-grinding by ball mill was done after the second heat treatment. Powders were also pressed to pellets at 3 tons of pressure for 2 minutes using a Carver press. The final heating was done at 725°C (at the rate of 120°C/h) for 24 hours.

For sample $Na_{1.5}Al_{0.5}Ti_{1.5}(PO_4)_3$ -B, same synthesis procedure was carried out but in a quartz tube with different starting materials. Stoichiometric quantities of Na_3PO_3, Al_2O_3 (aluminum oxide, α-phase, 99.98%), TiO_2 (Titanium (IV) oxide, rutile, 99.99% (metals basis)), $(NH_4)_2HPO_4$ (ammonium phosphate dibasic) were heated in silica tube to give the following overall reaction:

$$3/2\ Na_3PO_3 + 1/4\ Al_2O_3 + 3/2\ TiO_2 + 3/2\ (NH_4)_2HPO_4 \xrightarrow{\Delta} Na_{1.5}Al_{0.5}Ti_{1.5}(PO_4)_3\text{-B} + \text{gases}$$

2.1.2 $Li_{1.5}Al_{0.5}Ti_{1.5}(PO_4)_3$

$Li_{1.5}Al_{0.5}Ti_{1.5}(PO_4)_3$ is synthesized with Li_2CO_3, Al_2O_3 (Aluminum oxide, α-phase, 99.98%), TiO_2 (Titanium (IV) oxide, rutile, 99.99% (metals basis)), $(NH_4)_2HPO_4$ (ammonium phosphate dibasic) using the similar procedure.

$$3/4\ Li_2CO_3 + 1/4\ Al_2O_3 + 3/2\ TiO_2 + 3\ (NH_4)_2HPO_4 \xrightarrow{\Delta} Li_{1.5}Al_{0.5}Ti_{1.5}(PO_4)_3 + \text{gases}$$

2.1.3 ZrP_2O_7 precursor

ZrP_2O_7 was synthesized using starting materials of ZrO_2 and $NH_4H_2PO_4$. ZrO_2 was dried at 140°C for 24 hours. 15 wt% excess $NH_4H_2PO_4$ was added and starting materials were measured and ground using a mortar and pestle for 15 minutes. Mixtures were heated at 900°C for 10-20 hours. Both air and O_2 atmospheres were tried.

$$ZrO_2 + 2\ NH_4H_2PO_4 \xrightarrow{\Delta} ZrP_2O_7$$

2.2 Results and discussions

2.2.1 Synthesis from oxide and carbonate precursors

Oxide and carbonate starting materials (Li_2CO_3/Na_2CO_3, Al_2O_3, TiO_2, $(NH_4)_2HPO_4$) were firstly tried, but samples melted and stuck to corundum crucibles after the first heating. Little powder could be recovered and less for the next two heating processes. Quartz boat, Mo foil, gold foil and porcelain plate were alternatives to corundum crucibles. Out of those reaction containers, Mo foil and carbon crucible were used under N_2 atmosphere to avoid the oxidation of Mo and C.

However, all results in failure due to melting and phosphate loss. After those failed experiences, synthesis goes with more grinding, using activated TiO_2 instead of rutile TiO_2 and using a new precursor to avoid phosphate loss.

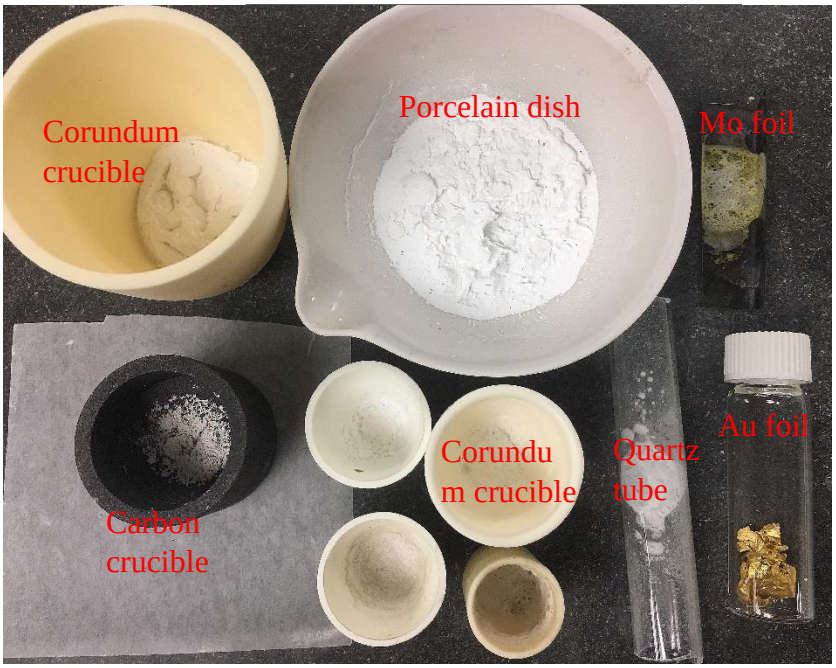

Figure 9. Ruined corundum crucibles, carbon crucible, porcelain dish, Mo boat, quartz tube and gold foil

2.2.2 Use of activated TiO_2 and $NaPO_3$

Using activated TiO_2 instead of conventional rutile TiO_2 is to enhance the reaction between things melting. Based on the decomposition and melting information of reagents, we can roughly suspect that the first heating at 350°C is to decompose $(NH_4)_2HPO_4$. The second heating at 650°C is for complete decomposition of Li_2CO_3, Na_2CO_3 and $(NH_4)_2HPO_4$.

Table 2. Decomposition and melting points of some reagents

Compounds	Decomposition temperature (°C)	Melting point (°C)
Li_2CO_3	650-900	723
Na_2CO_3	>400	851
$(NH_4)_2HPO_4$	70	155

From the X-ray diffraction pattern of activated TiO_2 in Figure 10, anatase TiO_2 peaks are observed. In Figure 10, the wider peak width of anatase TiO_2 than that of rutile alternatives which suggests that anatase TiO_2 has a much smaller particle size than rutile TiO_2, precursors that was originally used. During the synthesis of activated TiO_2, some isopropanol was added to slow down the hydrolysis process and slowly depositing got smaller anatase TiO_2 particles.

The use of activated TiO_2 resulted in much better powder than previous experiments, and over 90% products can be removed from corundum crucibles.

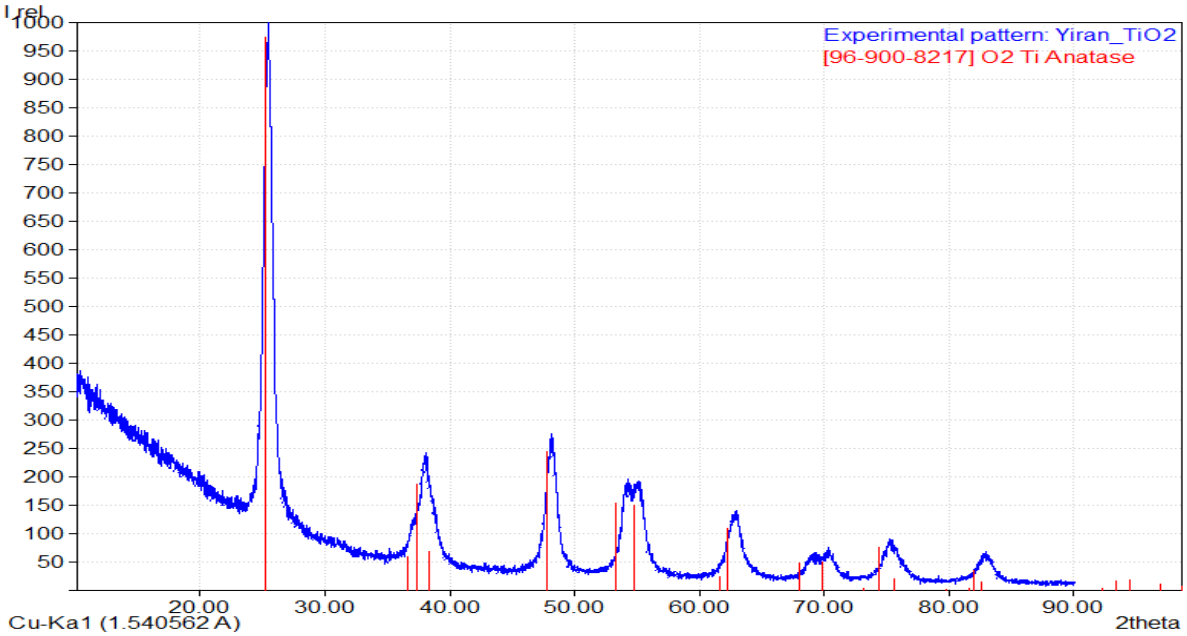

Figure 10. X-ray diffraction pattern of activated TiO_2

$NaPO_3$ was added as another P source. And rutile TiO_2 was used this time. Powders were obtained from this synthesis and Figure 10 shows the overlaid XRD patterns of two $Na_{1.5}Al_{0.5}Ti_{1.5}(PO_4)_3$ samples.

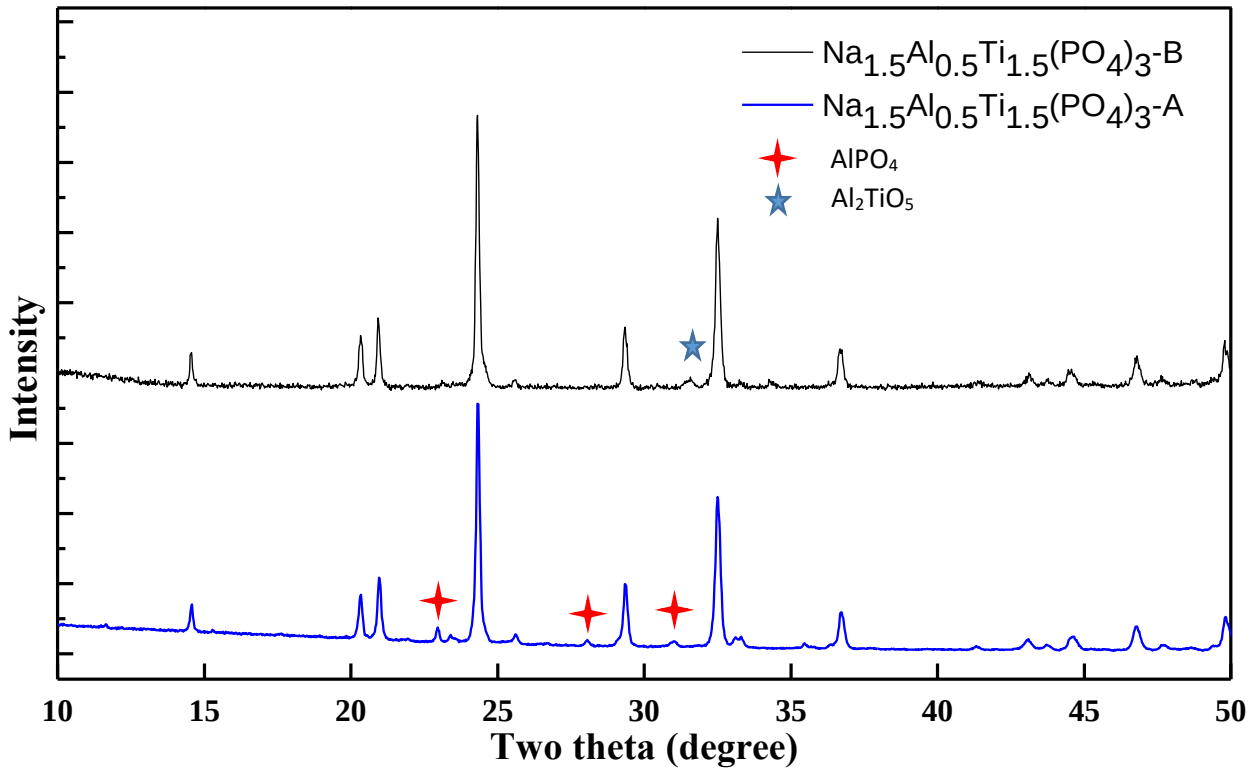

Figure 11. XRD patterns of two $Na_{1.5}Al_{0.5}Ti_{1.5}(PO_4)_3$ samples ($Na_{1.5}Al_{0.5}Ti_{1.5}(PO_4)_3$-A in blue and $Na_{1.5}Al_{0.5}Ti_{1.5}(PO_4)_3$-B in black)

From comparison of XRD patterns of two $Na_{1.5}Al_{0.5}Ti_{1.5}(PO_4)_3$ samples in Figure 11, some $AlPO_4$ and Al_2TiO_5 impurity phase were found. Berlinite $AlPO_4$ peaks (marked by red star) appears in $Na_{1.5}Al_{0.5}Ti_{1.5}(PO_4)_3$-A. And Al_2TiO_5 impurity phase was found in sample B. The starting materials of both two reactions were added in the stoichiometric amount. In addition, during these two experiments, temperatures of heating and time of grinding are all the same.

The XRD data of $Na_{1.5}Al_{0.5}Ti_{1.5}(PO_4)_3$ and $Li_{1.5}Al_{0.5}Ti_{1.5}(PO_4)_3$ indicated that they are crystalline solids with structure belonging to the R-3c NASICON structure type. Some berlinite $AlPO_4$ impurity peaks appeared.

Table 3. Refinement result of LATP

LATP (wt%)	**Berlinite $AlPO_4$ (wt%)**
97.34	2.66

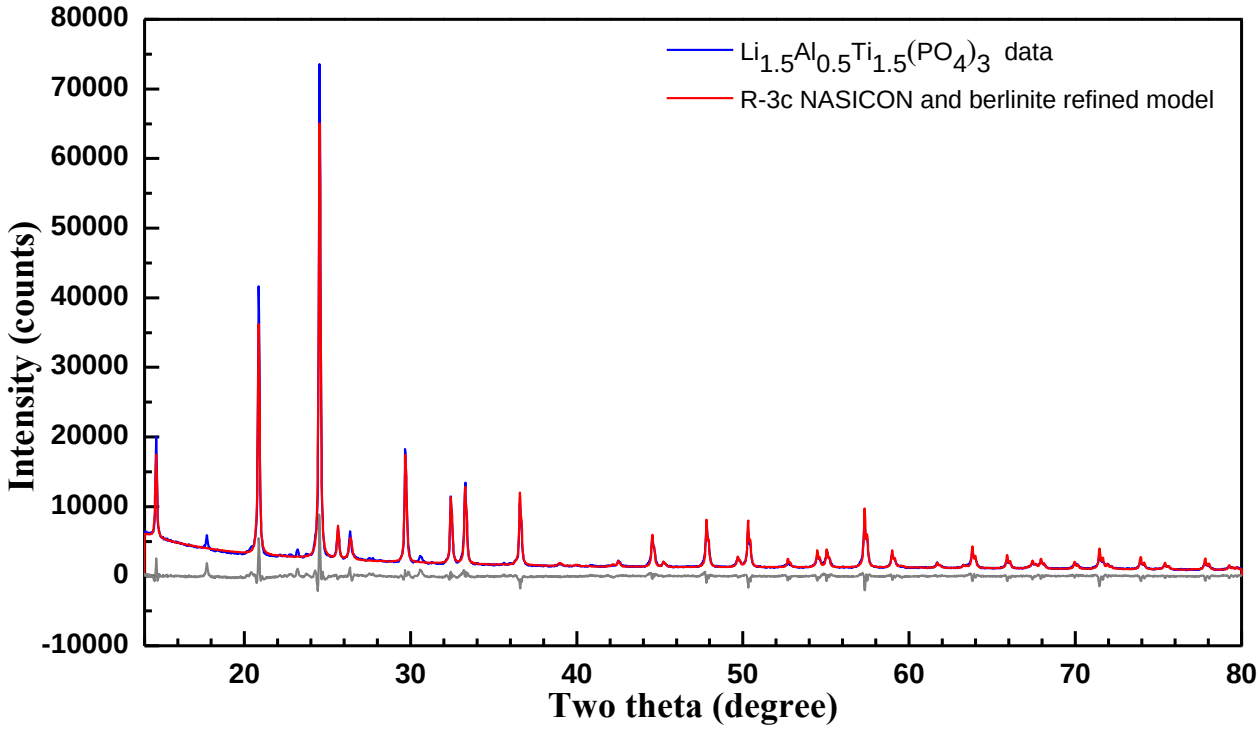

Figure 12. X-ray diffraction pattern and R-3c Rietveld refinement of $Li_{1.5}Al_{0.5}Ti_{1.5}(PO_4)_3$

For the synthesis section, many different crucibles and container were tried, such as molybdenum boat, quartz tube, carbon crucible, corundum crucible, porcelain dish, gold foil. In those efforts, carbon crucible and molybdenum boat should be used in inert gas atmosphere because carbon reacts with O_2 at over 460°C and weak oxidation of molybdenum starts at 300°C.

Most efforts failed because that samples reacted with crucibles and over 90% sample of the could cannot be removed from crucibles.

2.2.3 ZrP_2O_7 precursor

ZrP_2O_7 precursor was prepared for another kind of NASICON-type solid state electrolyte used in sodium batteries: $NaZr_2P_3O_{12}$. The expected reaction should be:

$$ZrP_2O_7 + NaPO_3 + ZrO_2 \xrightarrow{\Delta} NaZr_2P_3O_{12}.$$

ZrP_2O_7 precursors can be get from the reaction: $ZrO_2 + 2\ NH_4H_2PO_4 \xrightarrow{\Delta} ZrP_2O_7$.

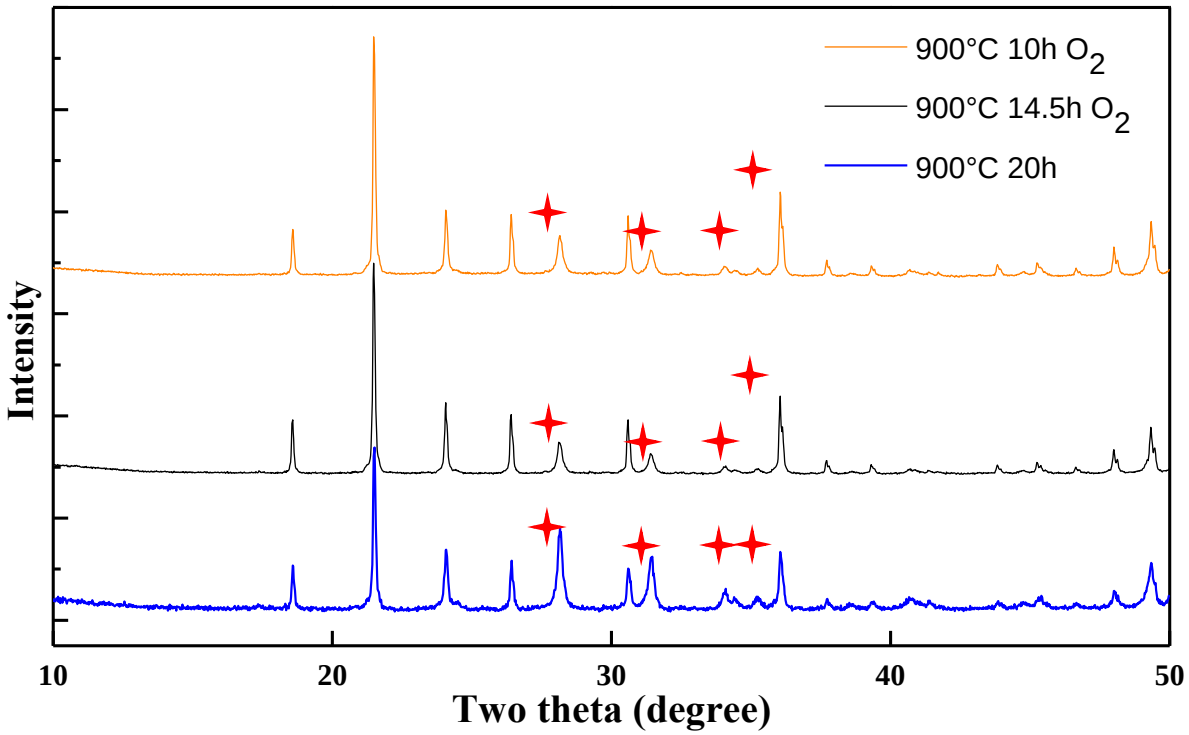

Figure 13. Overlaid patterns of ZrP_2O_7

Based on Figure 13 the XRD results of precursor ZrP_2O_7 synthesis, some ZrO_2 peaks were found. Although extra phosphate source $NH_4H_2PO_4$ was added and longer heating was held during the experiment, we can't see any improvement for this reaction.

Through the research of NASICONs synthesis, $Li_{1.5}Al_{0.5}Ti_{1.5}(PO_4)_3$ and $Na_{1.5}Al_{0.5}Ti_{1.5}(PO_4)_3$ were prepared and found they have R-3c space group. For $Na_{1.5}Al_{0.5}Ti_{1.5}(PO_4)_3$ synthesis, use of activated TiO_2 or $NaPO_3$ as a precursor can present samples from sticking to crucibles. Precursor ZrP_2O_7 could not be prepared as a single phase sample even when excess phosphous was added.

Chapter 3. Alpha-crystobalite $AlPO_4$

$AlPO_4$ is isoelectronic with Si_2O_4. Berlinite $AlPO_4$ looks like quartz and has a structure that is similar to quartz with Si replaced by Al and P in an order arrangement where the AlO_4 and PO_4 tetrahedra alternate. Correspondingly, berlinite $AlPO_4$ exhibits chirality and piezoelectric properties like quartz.[34] Alpha-cristobalite SiO_2 is an auxetic material, a material that has negative Poisson's ratio. Auxetic materials become thicker perpendicular to the applied force when stretched, which is opposite to normal materials. Based on the close relation between SiO_2 and $AlPO_4$, alpha-cristobalite $AlPO_4$ is expected to have a similar property like negative Poisson's ratio.

When heated, crystalline berlinite $AlPO_4$ converts to tridymite and cristobalite forms, and this also mirrors the behavior of silicon dioxide.[35] Alpha-cristobalite form $AlPO_4$ was synthesized for further mechanical properties test.

3.1 Experimental

3.1.1 Phase transformation

Alpha-cristobalite $AlPO_4$ powder samples were directly prepared by heating high purity purchased amorphous $AlPO_4$ at 1425°C-1500°C for several hours. Pellets of purchased powder were pressed in a half inch die at 2 tons of pressure for 2 minutes using a Carver press before heating.

3.1.2 Air quenching

Previous samples were carried out a second heating at 1100°C for 3 hours in box furnace. Pellets were taken out at 1100°C after heating treatment.

3.2 Results and discussions

3.2.1 Results from natural cooling

At the beginning, alpha-cristobalite form $AlPO_4$ sample was simply obtained from heating and natural cooling. Heating purchased $AlPO_4$ at 1350°C for 3h was first tried. Tridymite form $AlPO_4$ peaks appeared as a major impurity in the X-ray diffraction pattern. Based on its transformation diagram：

$$\text{Berlinite} \xleftrightarrow{815\pm4^\circ C} \text{Tridymite Form} \xleftrightarrow{1025\pm50^\circ C} \text{Cristobalite Form} \xleftrightarrow{>1600^\circ C} \text{Fused } AlPO_4$$

$$A \xleftrightarrow{586\pm2^\circ C} \beta \qquad \alpha \xleftrightarrow{908\pm3^\circ C} \beta_1 \xleftrightarrow{945^\circ C} \beta_2 \qquad \alpha \xleftrightarrow{1240\pm5^\circ C} \beta$$

Tridymite $AlPO_4$ forms above 815°C and transforms to alpha-cristobalite form at 1025°C. But no reported information on how long it would take. To figure out if those tridymite form $AlPO_4$ are from uncompleted phase transformation or not, both extending heating time and raising temperature were tried.

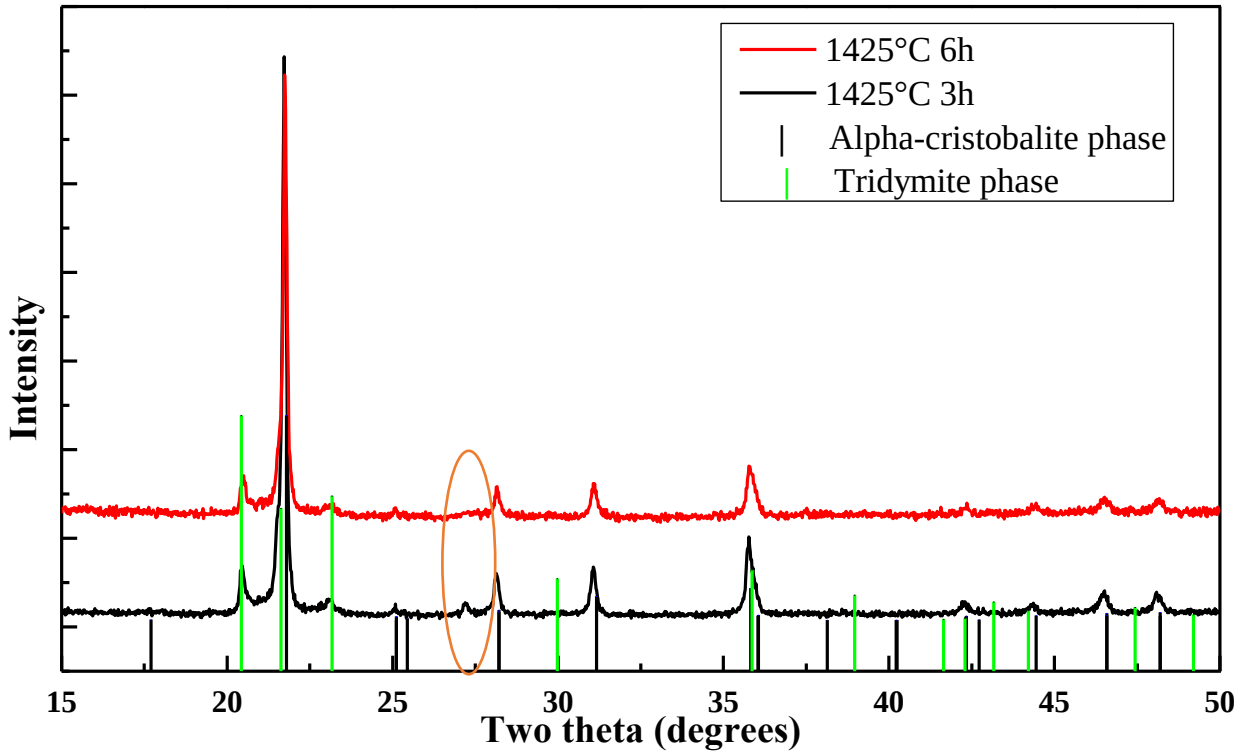

Figure 14. Fit XRD patterns of samples at 1425°C

Figure 14 shows the overlaid XRD patterns of samples prepared at 1425°C but differs from 3 hours to 6 hours. Black lines represent the ideal cristobalite $AlPO_4$ phase and green lines show the tridymite form $AlPO_4$. A clear difference located at around 27.3°. 1425°C 6h curve in red has fewer impurity peaks than 1425°C 3h in black.

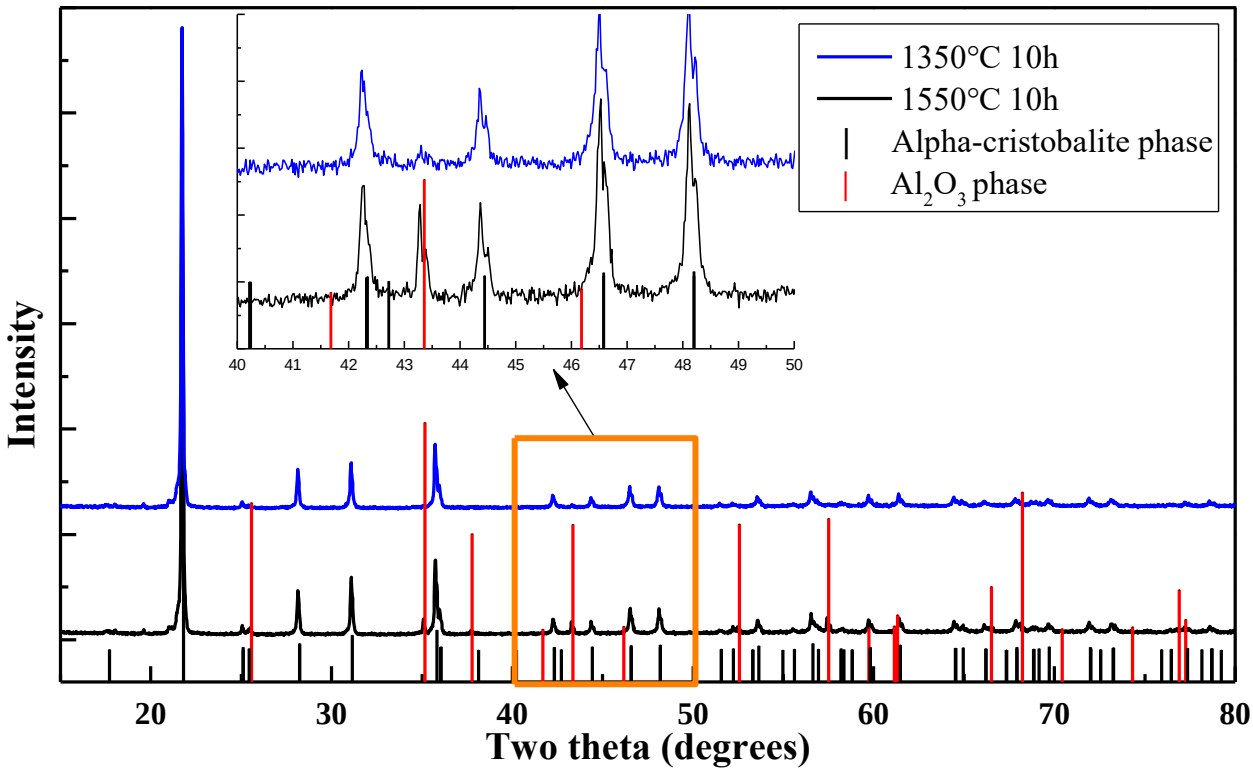

Figure 15. Overlaid XRD patterns of samples heating for 10h

Figure 15 shows the XRD results of samples from both 10 hours but different temperatures. In Figure 15, red lines represent Al_2O_3 corundum phase, and black lines represent the ideal cristobalite $AlPO_4$ phase. From the zoomed graph, we can clearly observe that in both conditions there is more Al_2O_3 at a higher temperature. In all synthesis, the starting material is purchased $AlPO_4$ but no Al_2O_3 including. In this case, it may because phosphorus lost when extending the heating time.

Out of those results, the best data is the one heating at 1425°C for 6 hours. It was refined with alpha-cristobalite and tridymite form $AlPO_4$ as is shown in Figure 16. The refinement also resulted in the weight percentage of cristobalite form and tridymite form $AlPO_4$, which is 68.75 wt%: 31.25 wt%.

Table 4. Refienment result of AlPO4 sample from natural cooling

Cristobalite (wt%)	Tridymite (wt%)
68.75	31.25

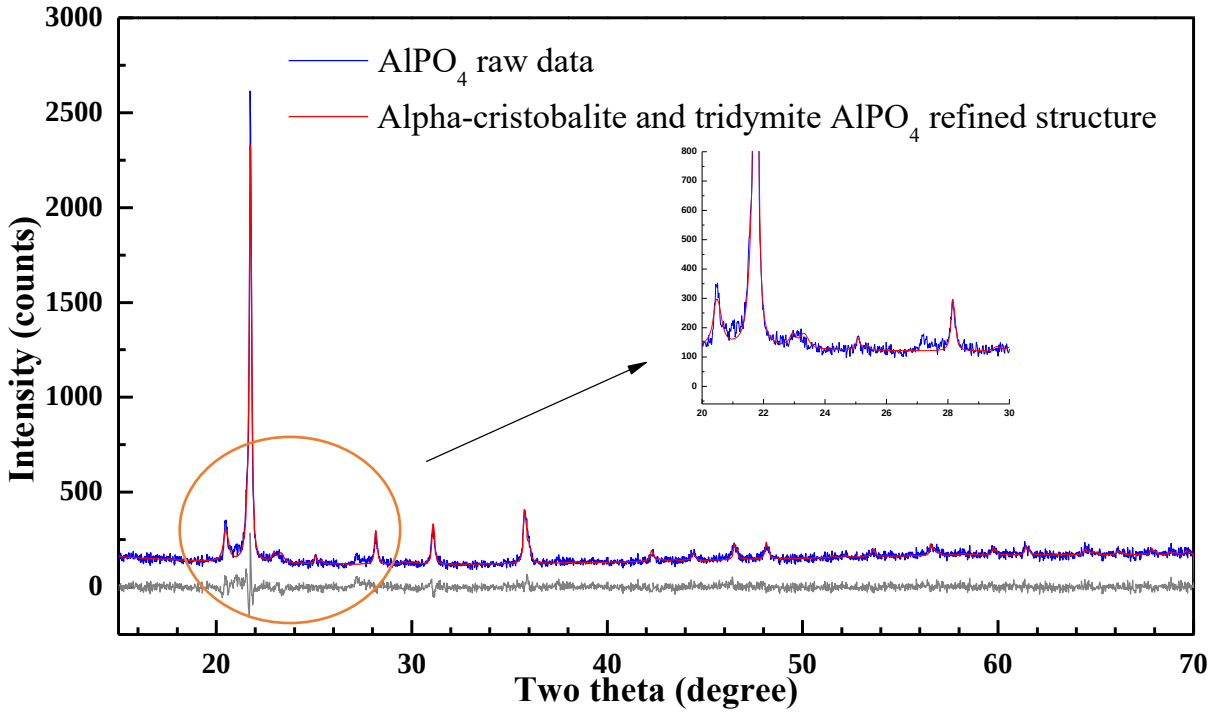

Figure 16. X-ray diffraction pattern of natural cooling $AlPO_4$ sample raw data and cristobalite form and tridymite form $AlPO_4$ refined structure

3.2.2 Air quenching

Taking the phase transformation diagram into consideration, at the range of 815°C-1025°C, it's a reasonable temperature to form tridymite form $AlPO_4$. Tridymite form $AlPO_4$ might form during the cooling stage. To avoid that happens, air quenching fast cooling might help.

Figure 16 shows the refined result of air quenching from 1100°C. Both fix are refined using same models. Particularly from the zoomed inset, we can see air quenched sample better matches the red curve and has fewer tridymite peaks.

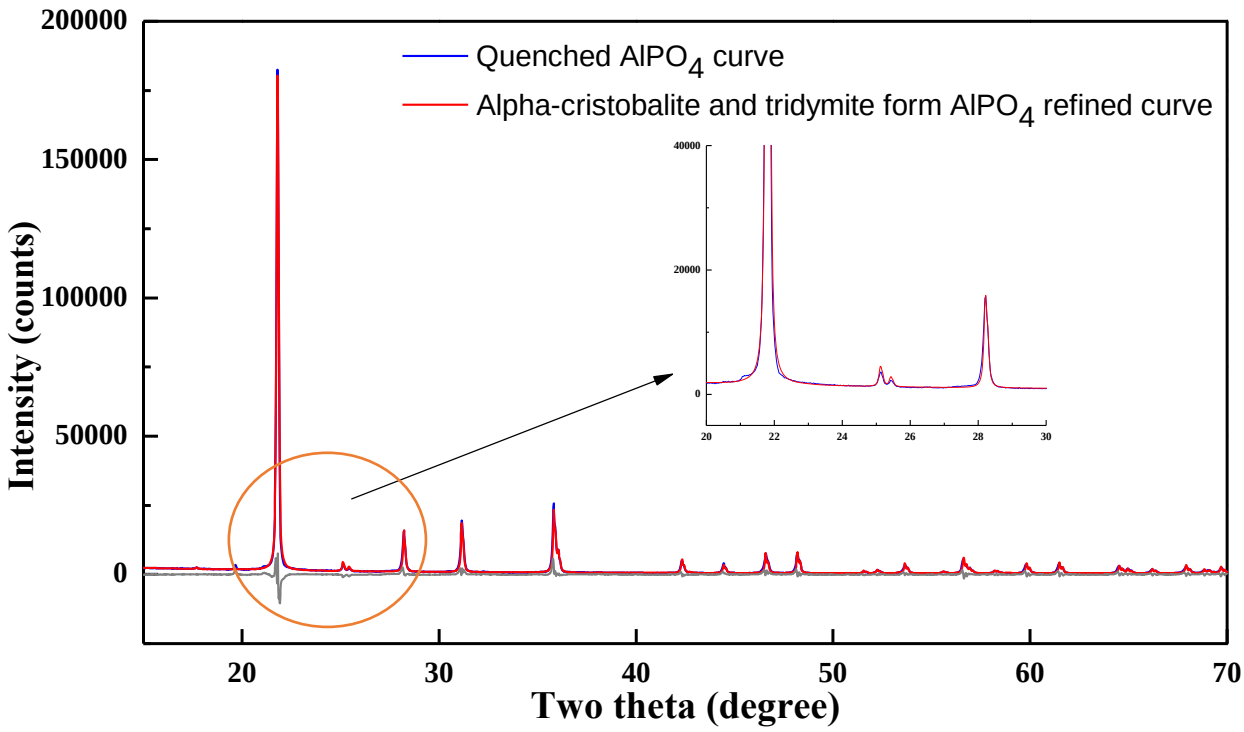

Figure 17. X-ray diffraction pattern and $C222_1$ Rietveld refinement of $AlPO_4$

The refinement shows there are 99.64 wt% cristobalite and 0.36 wt% tridymite $AlPO_4$. It's clear that quenching helps to reduce the impurities.

Table 5. Content of cristobalite and tridymite form $AlPO_4$ before and after air quenching

	Cristobalite (wt%)	**Tridymite (wt%)**
Natural cooling	68.75	31.25
Air quenching	99.64	0.36

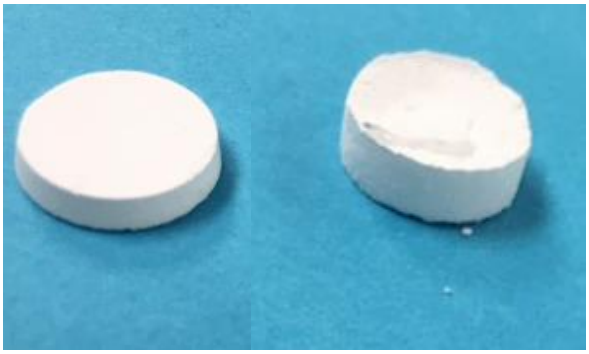

Figure 18. $AlPO_4$ pellets

Pellets were pressed under 2 tons pressure are not yet good enough to get further results from resonant ultrasound spectroscopy and tensile tests because they are not dense enough. Most pellets were fragile but much denser after calcination. Figure 18 shows the cracks on those imperfect pellets, although they have been heated.

Chapter 4. Conclusions and future work

4.1 NASICON

During this work, $Na_{1.5}Al_{0.5}Ti_{1.5}(PO_4)_3$, $Li_{1.5}Al_{0.5}Ti_{1.5}(PO_4)_3$, and ZrP_2O_7 powders were synthesized. The use of Na_3PO_3 or activated TiO_2 can efficiently avoid powder sticking to corundum crucibles, after fully mixing and grinding of precursors. ZrP_2O_7 precursors synthesis didn't show any improvement by changing calcination time and temperature.

$Na_{1.5}Al_{0.5}Ti_{1.5}(PO_4)_3$, $Li_{1.5}Al_{0.5}Ti_{1.5}(PO_4)_3$ are worth doing further research on its application on solid state electrolyte.

4.2. Alpha-cristobalite $AlPO_4$

Over 99% pure alpha-cristobalite $AlPO_4$ powder was successfully synthesized based on phase transformation and quenching process. But for the test of its mechanical properties like elasticity, it requires the sample dense enough. Several ideas can be tried in the future.

Single crystal growth. Some research has been done on single crystal growth for similar composition. Flux method and hydrothermal method are worth trying. Higher pressure press like using hydrostatic pressure press. Using binder, many kinds of binders could be added when preparing pellets, like PVA (Polyvinyl Alcohol) or oleic acid.

References

1. Wright, P. V. (1975). Electrical conductivity in ionic complexes of poly (ethylene oxide). Polymer International, 7(5), 319-327.
2. Wagh, A. S., & Jeong, S. Y. (2003). Chemically bonded phosphate ceramics: I, a dissolution model of formation. Journal of the American Ceramic Society, 86(11), 1838-1844.Vast, P. (1993). Bonding between metals and multicomponent phosphate based ceramic-glass. Application to the enamelling of nickel and titanium. Le Journal de Physique IV, 3(C7), C7-1383.
3. Armand, M. B.; Chagbano, J. M.; Duclot, M. J. In Fast Ion Transport in Solid; Vashishta, P., Mundy, J. N., Shenoy, G. K., Eds.; Elsevier N Holland: New York, 1979; p131
4. Nishimoto, A., Watanabe, M., Ikeda, Y., & Kohjiya, S. (1998). High ionic conductivity of new polymer electrolytes based on high molecular weight polyether comb polymers. Electrochimica acta, 43(10), 1177-1184.
5. Goodenough, J. B., & Kim, Y. (2011). Challenges for rechargeable batteries. Journal of Power Sources, 196(16), 6688-6694.
6. Batteries, L. (2004). Science and Technology. Eds Nazri G.-A., Pistoia G. Boston: Kluwer Academic, 1.
7. Takada, K., Aotani, N., & Kondo, S. (1993). Electrochemical behaviors of Li+ ion conductor, Li_3PO_4-Li_2S-SiS_2. Journal of power sources, 43(1), 135-141.
8. Machida, N., Maeda, H., Peng, H., & Shigematsu, T. (2002). All-Solid-State Lithium Battery with $LiCo_{0.3}Ni_{0.7}O_2$ Fine Powder as Cathode Materials with an Amorphous Sulfide Electrolyte. Journal of the Electrochemical Society, 149(6), A688-A693.
9. Nagata, K., & Nanno, T. (2007). All solid battery with phosphate compounds made through sintering process. Journal of Power Sources, 174(2), 832-837.
10. Goodenough, J. B., HY-P. Hong, and J. A. Kafalas. "Fast Na^+-ion transport in skeleton structures." Materials Research Bulletin 11.2 (1976): 203-220.
11. Anantharamulu, N., Rao, K. K., Rambabu, G., Kumar, B. V., Radha, V., & Vithal, M. (2011). A wide-ranging review on NASICON-type materials. Journal of materials science, 46(9), 2821-2837.
12. Delmas, C., Nadiri, A., & Soubeyroux, J. L. (1988). The nasicon-type titanium phosphates $ATi_2(PO_4)_3$ (A= Li, Na) as electrode materials. Solid State Ionics, 28, 419-423.
13. Rao, G. S., Varadaraju, U. V., Thomas, K. A., & Sivasankar, B. (1987). Metal atom incorporation studies on the phases with NZP structure: $NbTiP_3O_{12}$. Journal of Solid State Chemistry, 70(1), 101-107.
14. Berry, F. J., Tyrer, A. A., & Tyrer, E. C. (1990). Iron-57, tin-119, and antimony-121 mössbauer spectroscopic investigations of metal atom incorporation into the oxide $NbTiP_3O_{12}$. Hyperfine Interactions, 53(1-4), 297-303.
15. Berry, F. J., Greaves, C., & Marco, J. F. (1992). The structural characterization of $Sn_{0.5}NbTiP_3O_{12}$ and $Fe_{0.33}NbTiP_3O_{12}$. Journal of Solid State Chemistry, 96(2), 408-414.
16. Berry, F. J., Marco, J. F., & Vithal, M. (1994). Iron-57 Mössbauer spectroscopic studies of materials of composition Fe x $NbTiP_3O_{12}$: materials with low concentrations of iron and the effects of treatment in air. Hyperfine Interactions, 83(1), 351-355.
17. Alamo, J., & Roy, R. (1984). ULTRALOW-EXPANSION CERAMICS IN THE SYSTEM Na_2O-$ZrO_2P_2O_5$-SiO_2. Journal of the American Ceramic Society, 67(5).
18. Muller, O., & Roy, R. (1974). The major ternary structural families. Springer.
19. https://en.wikipedia.org/wiki/Auxetics

20. Lakes, Roderic. "Foam structures with a negative Poisson's ratio." Science 235 (1987): 1038-1041.
21. Kimizuka, Hajime, et al. "Molecular Dynamics Analysis of Negative Poisson Ratios over the α-β Transition in Cristobalite, SiO_2." Progress of Theoretical Physics Supplement 138 (2000): 229-233.
22. Mooney, R. C. (1956). The crystal structure of aluminium phosphate and gallium phosphate, low-cristobalite type. Acta Crystallographica, 9(9), 728-734.
23. Wood, I. G., Thompson, P., & Matthewman, J. C. (1983). A crystal structure refinement from Laue photographs taken with synchrotron radiation. Acta Crystallographica Section B: Structural Science, 39(5), 543-547.
24. Tucker, M. G., Keen, D. A., & Dove, T. (2001). A detailed structural characterization of quartz on heating through the α− β phase transition. Mineralogical Magazine, 65(4), 489-507.
25. Beck, Warren R. "Crystallographic inversions of the aluminum orthophosphate polymorphs and their relation to those of silica." Journal of the American Ceramic Society 32.4 (1949): 147-151.
26. De Biasi, R. S. (1980). ESR of V^{4+} ions alpha-cristobalite $AlPO_4$. Journal of Physics C: Solid State Physics, 13(33), 6235.
27. Giacovazzo, C. (2002). Fundamentals of crystallography (Vol. 7). Oxford university press, USA.
28. París, M. A., & Sanz, J. (1997). Structural changes in the compounds $LiM_2^{IV}(PO_4)_3$ (M^{IV}= Ge, Ti, Sn, and Hf) as followed by ^{31}P and ^{7}Li NMR. Physical Review B, 55(21), 14270.
29. Li, S. C., Cai, J. Y., & Lin, Z. X. (1988). Phase relationships and electrical conductivity of $Li_{1+x}Ge_{2-x}Al_xP_3O_{12}$ and $Li_{1+x}Ge_{2-x}Cr_xP_3O_{12}$ systems. Solid State Ionics, 28, 1265-1270.
30. Aono, H., Sugimoto, E., Sadaoka, Y., Imanaka, N., & Adachi, G. Y. (1990). Ionic conductivity of solid electrolytes based on lithium titanium phosphate. Journal of the electrochemical society, 137(4), 1023-1027.
31. Ado, K., Saito, Y., Asai, T., Kageyama, H., & Nakamura, O. (1992). Li^+-ion conductivity of $Li_{1+x}M_xTi_{2-x}(PO_4)_3$ (M: Sc^{3+}, Y^{3+}). Solid state ionics, 53, 723-727.
32. Aatiq, A., Ménétrier, M., Croguennec, L., Suard, E., & Delmas, C. (2002). On the structure of $Li_3Ti_2(PO_4)_3$. Journal of Materials Chemistry, 12(10), 2971-2978.
33. McDaniel, A. H., Ihlefeld, J. F., & Bartelt, N. C. (2015). *Ion-Conduction Mechanisms in NaSICON-Type Membranes for Energy Storage and Utilization* (No. SAND--2015-8531). Sandia National Laboratories (SNL-CA), Livermore, CA (United States); Sandia National Laboratories, Albuquerque, NM (United States).
34. Motchany, A. I., & Chvanski, P. P. (2001, January). Crystal growth of an α-quartz like piezoelectric material, berlinite. In Annales de Chimie Science des Materiaux (Vol. 26, No. 1, pp.199-208). No longer published by Elsevier.
35. Greenwood, Norman N.; Earnshaw, Alan (1997). Chemistry of the Elements (2nd ed.). Butterworth-Heinemann. ISBN 0-08-037941-9.